Optimization of Spin-Wave Propagation with Enhanced Group Velocities by Exchange-Coupled Ferrimagnet-Ferromagnet Bilayers

K. An,[1,*] V.S. Bhat,[1] M. Mruczkiewicz,[2] C. Dubs,[3] and D. Grundler[1,4]

[1]*Laboratory of Nanoscale Magnetic Materials and Magnonics, Institute of Materials (IMX), School of Engineering, École Polytechnique Fédérale de Lausanne (EPFL), 1015 Lausanne, Switzerland*
[2]*Institute of Electrical Engineering, Slovak Academy of Sciences, 841 04 Bratislava, Slovakia*
[3]*INNOVENT e.V. Technologieentwicklung, Prüssingstraße 27B, D-07745 Jena, Germany*
[4]*Institute of Microengineering (IMT), School of Engineering, École Polytechnique Fédérale de Lausanne (EPFL), 1015 Lausanne, Switzerland*

(Received 25 July 2018; revised manuscript received 17 December 2018; published 27 March 2019)

We report broadband spectroscopy and numerical analysis by which we explore propagating spin waves in a magnetic bilayer consisting of a 23-nm thick permalloy film deposited on 130-nm thick $Y_3Fe_5O_{12}$. In the bilayer, we observe a characteristic mode that exhibits a considerably larger group velocity at a small in-plane magnetic field than both the magnetostatic and perpendicular standing spin waves. Using the finite element method, we confirm the observations by simulating the mode profiles and dispersion relations. They illustrate the hybridization of spin-wave modes due to exchange coupling at the interface. The high-speed propagating mode found in the bilayer can be utilized to configure multifrequency spin-wave channels enhancing the performance of spin-wave-based logic devices.

DOI: 10.1103/PhysRevApplied.11.034065

I. INTRODUCTION

In the field of spintronics, building blocks for low-power consuming logic and data processing devices might exploit spin waves [1–3]. Studies on the generation, manipulation, and detection of spin waves have already evolved into a broader research field called magnonics [4–8]. One of the immediate challenges is the generation of short-waved spin waves, which are particularly important for miniaturizing devices [9,10]. Here, a long propagation distance and a high group velocity of spin waves are desired. In a magnetic thin film, perpendicular standing spin waves (PSSWs) reflect exchange-dominated modes, which are quantized between the top and bottom surfaces. For a magnetic film with a thickness of 130 nm, the first order PSSW (PSSW1) corresponds to a large wave vector of $k_{\mathrm{perp}} = 24.2$ rad/μm pointing perpendicular to the film. When PSSWs acquire a small in-plane wave vector component k_i in, for example, ferrimagnetic yttrium iron garnet $Y_3Fe_5O_{12}$ (YIG), the modes are known to exhibit a small group velocity, contradicting fast and efficient signal transmission. Conventional microstructured microwave antennas allow one to transfer k_i on the order of 1 rad/μm, and if integrated to a planar film, are known to excite PSSW only weakly [11]. Recently, undulation of a $Co_{40}Fe_{40}B_{20}$ film was shown to allow for efficient PSSW excitation within the same film [12]. For planar YIG, it was reported that top layers of either Co [13] or $Co_{40}Fe_{40}B_{20}$ [14] enhanced PSSW amplitudes considerably. This was attributed to interfacial exchange-mediated spin-transfer torque. Bilayers composed of permalloy (Py) and YIG have also been studied [15–17] concerning magnetic resonances and coupling at the interface. However, the propagation characteristics, such as signal transmission and group velocities, have not been analyzed yet.

Here, we explore propagating spin waves excited in bilayers of Py and YIG. In addition to the magnetostatic surface spin wave (MSSW), we detect a further spin-wave mode with an unexpectedly high group velocity (v_g) of about 4500 m/s in a small in-plane magnetic field $\mu_0 H$ of 4 mT. Finite-element modeling of the YIG/Py bilayer attributes the high v_g to a PSSW-like hybridized mode with a total wave vector $k_{\mathrm{tot}} = \sqrt{k_{\mathrm{perp}}^2 + k_i^2} = 24.2$ rad/μm. Originating from a PSSW, the hybrid mode resides at a different frequency compared to the MSSW with $k_{\mathrm{tot}} = k_i$. Our observation allows one to configure multifrequency magnonic devices offering spin-wave modes with high group velocities.

II. EXPERIMENTAL AND NUMERICAL METHODS

A single-crystalline YIG film with a thickness of 130 nm is grown by liquid phase epitaxy on a (111) gadolinium gallium garnet substrate [18]. A 23-nm thick Py ($Ni_{81}Fe_{19}$) film is deposited on the YIG using electron

*kyongmo.an@epfl.ch

beam evaporation. As a control sample, a nominally identical YIG film without Py is explored. Subsequently, a 34-nm thick SiO_2 layer is deposited to provide electrical insulation and allow for the integration of two parallel coplanar wave guides (CPWs). They consist of 180-nm thick gold on a 5-nm thick adhesion layer of Ti. Both the YIG and YIG/Py samples are shaped to parallelograms using ion-beam etching. This shape avoids the formation of standing spin waves in the lateral direction. The signal and ground lines of CPWs are 3.3-μm wide and exhibit an edge-to-edge separation of 2.7 μm. The distance d between two signal lines amounts to 30 and 18 μm for the YIG and YIG/Py samples, respectively. The in-plane wave vector k_i most efficiently excited by the CPWs is determined to be 0.5 rad/μm via Fourier transforming the in-plane component of the microwave field [19]. A microwave power of -5 dBm is provided by the vector network analyzer (VNA), and transmission signals from CPW1 to CPW2 ($S21$) are recorded. A schematic of the measurement geometry is shown in Fig. 1(a). In our experiment, the spin wave propagates along the $-x$ direction, the y axis is perpendicular to the film, and the magnetic field is applied along the z axis. To enhance the signal-to-noise ratio, spectra measured at two slightly different magnetic fields are subtracted from each other. The subtracted signal $\Delta S21$ is displayed in color-coded graphs as shown in Figs. 1(b) and 1(c). Considering the phase-sensitive detection of the VNA, the signal $S21$ at the receiver port experiences a phase accumulation of $k_i d$ due to spin waves propagating between CPW1 and CPW2. Spin waves with different k_i arrive at the receiver port with different phases, resulting in an oscillating amplitude [as shown in Figs. 1(d)–1(g)]. A phase difference of 2π is accumulated when the difference in wave vectors satisfies the relation $2\pi = d\Delta k_i$. Approximating the spin-wave-dispersion relation to be linear in k_i, we write $v_g = 2\pi df/dk \approx 2\pi \Delta f/\Delta k$. The group velocity is obtained by $v_g = d\Delta f$ [20,21].

Using the finite element method COMSOL, we solve the Landau–Lifshitz equation (without damping term). For YIG, we use the exchange constant $A_{\mathrm{YIG}} = 3.7 \times 10^{-12}$ J/m [22], the gyromagnetic ratio $\gamma_{\mathrm{YIG}}/(2\pi) = 28$ GHz/T, and a magnetization value of $\mu_0 M_{\mathrm{YIG}} = 0.1835$ T extracted from a separately conducted magnetic resonance measurement. For Py, we use $A_{\mathrm{Py}} = 1.03 \times 10^{-11}$ J/m [23], $\gamma_{\mathrm{Py}}/(2\pi) = 29.4$ GHz/T [24], and $\mu_0 M_{\mathrm{Py}} = 1.018$ T [24]. We impose a periodic boundary condition along the x axis with a unit cell size of 20 nm. Considering the periodic boundary condition, the dynamic components of magnetization, m_x and m_y, take the form of a plane wave, that is, $m_j(x,y,t) = m_j(y)e^{-i(kx-\omega t)}$ with $j = x,y$. The wave vector k is parametrically swept within the simulation to obtain the dispersion relation. Two 1-nm thick intermediate layers are introduced at the interface to simulate the interfacial exchange coupling between YIG and Py. We use the same magnetic parameters corresponding to their parent layers with an interfacial exchange constant defined by $A_{\mathrm{int}} \equiv (A_{\mathrm{YIG}} + A_{\mathrm{Py}})/2$.

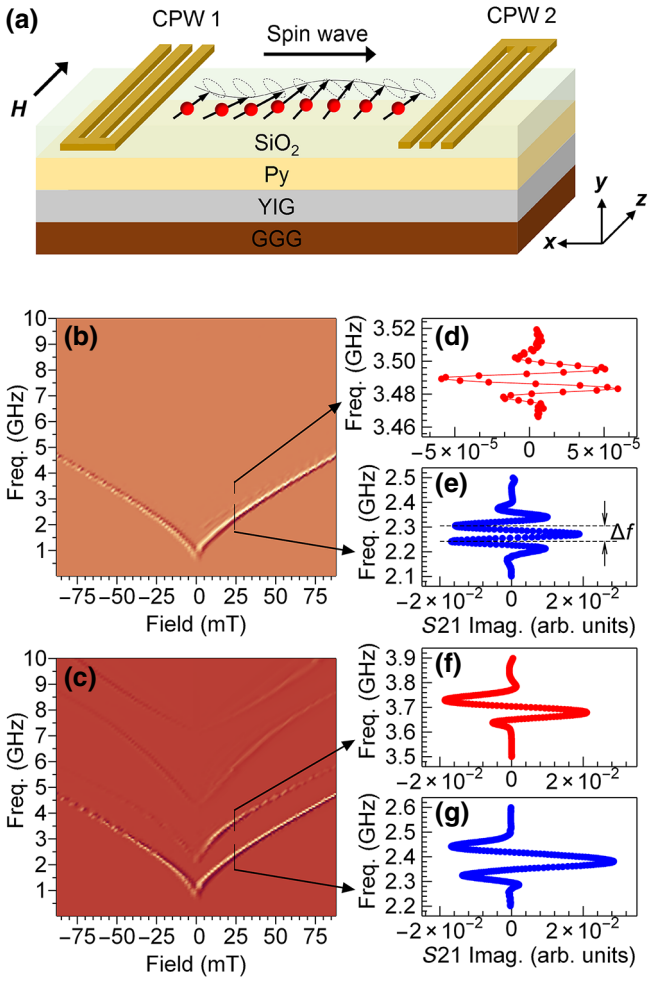

FIG. 1. (a) Schematics of sample and transmission measurement geometries. Measured spin-wave transmission signal from (b) bare YIG film and (c) YIG/Py bilayer. The arrows indicate where the linecuts of spectra are taken. The linecuts (d) and (e) represent the PSSW1 and MSSW in bare YIG at 24 mT. Similarly, the linecuts (f) and (g) represent the PSSW1 and MSSW in the YIG/Py bilayer at 24 mT. The separation between adjacent maximum frequencies are defined as Δf. An example of such a frequency spacing is shown in (e).

III. RESULTS

Transmission spectra (imaginary part of $\Delta S21$) obtained from the bare YIG film and the YIG/Py bilayer are shown in Figs. 1(b) and 1(c), respectively. Compared to the bare YIG [Fig. 1(b)], more spin-wave branches are visible in the YIG/Py bilayer [Fig. 1(c)]. The lowest and most prominent branch in each graph is attributed to the MSSW in YIG. The signal strength is larger for a positive field than for a negative field, which is attributed to nonreciprocity

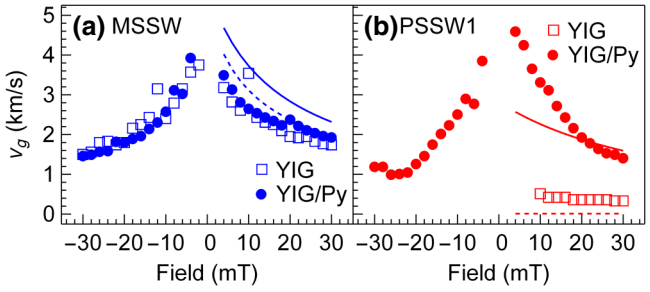

FIG. 2. Field dependencies of group velocities for (a) MSSW and (b) PSSW1, both attributed to YIG. The solid (dashed) lines are simulation results for the YIG/Py (bare YIG) sample. The PSSW1 group velocity is not extracted for negative magnetic field due to a low signal-to-noise ratio.

[25]. In Fig. 1(c), a second branch is found to be residing at a larger frequency compared to the MSSW. The higher frequency is consistent with the PSSW1 in YIG as will be discussed later. Above about 6 GHz, we observe two further modes for the YIG/Py bilayer. Their frequencies are close to both the MSSW in Py and the second-order PSSW in YIG. An anticrossing at about 53 mT in Fig. 1(c) is attributed to the coupling between these two modes. The anticrossing behavior has been studied extensively in other bilayer systems and we do not discuss this aspect any further [13,14]. In the following, MSSW and PSSW1 refer to the modes attributed to the YIG unless otherwise stated.

Next, we extract v_g from the two lowest lying branches in Figs. 1(b) and 1(c). Overall, v_g is found to decrease with increasing absolute value of the magnetic field as shown in Fig. 2. Specifically, at 24 mT, Δf_{MSSW} for bare YIG and YIG/Py is equal to 65 MHz [Fig. 1(e)] and 117 MHz [Fig. 1(g)], respectively. Considering the relevant signal-to-signal line separation d, we obtain the corresponding v_{MSSW} of 1950 and 2100 m/s for the bare YIG and YIG/Py, respectively, which are similar [Fig. 2(a)]. $\Delta f_{\mathrm{PSSW1}}$ for the bare YIG and YIG/Py corresponds to 12 and 91 MHz, which provides $v_{\mathrm{PSSW1}} = 360$ m/s and 1640 m/s, respectively. Here, YIG/Py shows v_{PSSW1}, which is larger by a factor of 4.6 compared to that of bare YIG. At a smaller field of 10 mT, the enhancement factor for v_g amounts to 6.5 [Fig. 2(b)]. We note that Py is not in magnetic resonance in the frequency regime. The ferromagnetic resonance frequency of Py is about 4.6 GHz at 24 mT [Fig. 3(e)] and v_g of Py is between 5 and 7 km/s [Fig. 3(j)]. The signal strength of PSSW1 in YIG/Py is more than three orders of magnitude larger than that of the bare YIG [Figs. 1(f) and 1(d), respectively]. The results show that both the group velocity and excitation amplitude of PSSW1 are enhanced by the presence of the Py top layer.

The amplitudes of MSSWs are similar for YIG and YIG/Py [Figs. 1(e) and 1(g), respectively]. Based on the amplitudes, we can estimate the decay lengths for MSSWs in YIG and YIG/Py at 24 mT (see Supplemental Material [26]), [27]. The analysis suggests that the Py layer

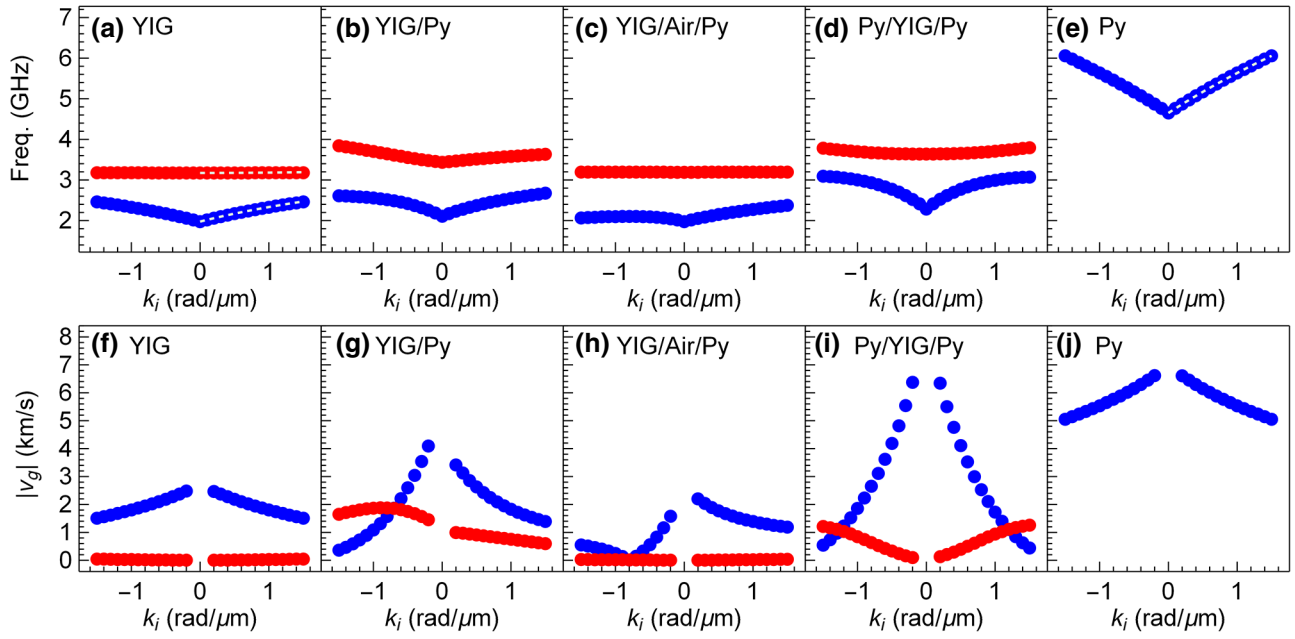

FIG. 3. Simulated dispersion relations for (a) YIG, (b) YIG/Py, (c) YIG/Air/Py, (d) Py/YIG/Py, and (e) Py at 24 mT. Corresponding group velocities for (f) YIG, (g) YIG/Py, (h) YIG/Air/Py, (i) Py/YIG/Py, and (j) Py as a function of in-plane wave vector k_i. The thicknesses of YIG and Py used in the simulations are 130 and 23 nm, respectively. The blue (red) symbols represent the MSSW (PSSW1). The dashed lines in (a) and (e) are calculated following the analytic formula in Ref. [28] for unpinned spins at boundaries.

deposited on top of YIG does not decrease the decay length.

IV. SIMULATION

In Figs. 3(a) and 3(b), we show numerically calculated dispersion relations for MSSW and PSSW1 of bare YIG and YIG/Py samples at 24 mT. The solid lines in Fig. 3(a) reflect the analytic formulas of Ref. [28] and they are consistent with the simulated frequencies. It is found that the top Py layer shifts the spin-wave frequencies of YIG to larger values and makes branches asymmetric with respect to the in-plane wave vector component k_i. In Fig. 3(f), we depict the calculated v_{MSSW} (blue symbols) and v_{PSSW1} (red symbols) of the bare YIG film. The v_{PSSW1} is more than an order of magnitude smaller compared to v_{MSSW}. This is no longer true for the YIG/Py sample [Fig. 3(g)]. Here, v_{PSSW1} (red symbols) has increased by roughly an order of magnitude. In addition, v_{MSSW} is larger compared to that of the bare YIG for small wave vectors. The group velocities of YIG/Py calculated for $k_i = -0.5$ rad/μm are $v_{\mathrm{PSSW1}} = 1750$ m/s and $v_{\mathrm{MSSW}} = 2600$ m/s. These values are in good agreement with the measured values considering that the simulation is performed based on the assumed parameters and boundary conditions.

In addition, we simulate the case where the exchange coupling between YIG and Py is eliminated by replacing the 2-nm thick intermediate layer with an air layer. With the insertion of an air layer, the MSSW dispersion is still asymmetric while the dispersion of PSSW1 is flat. The corresponding velocity v_{PSSW1} is similar to that of bare YIG [Fig. 3(h)]. The result indicates that the direct contact between YIG and Py with exchange coupling is essential to observe an enhanced group velocity of PSSW1. To further investigate the enhancement mechanism, we simulate a Py/YIG/Py layer. Here, the exchange coupling induces forced oscillations in both Py layers, however, the dynamic dipolar field from the Py layers is expected to exhibit a symmetric profile. In Fig. 3(i), we show the calculated group velocities. v_{PSSW1} increases linearly with k. It approaches zero for $k \to 0$, consistent with the exchange-dominated dispersion relation ($A_{\mathrm{ex}}k^2$). These characteristics suggest that the exchange effect is dominant for the Py/YIG/Py layer. They are not observed for the asymmetrically designed bilayer YIG/Py [red dots in Fig. 3(g)] where v_{PSSW1} is finite for $k \to 0$. In Fig. 3(g), the group velocity is finite for $k \to 0$, showing that the asymmetry of the dynamic dipolar field is the dominant effect for a greater v_{PSSW1} in YIG/Py.

Using simulated dispersion relations, we calculate the group velocity at each magnetic field (Fig. 2). The solid and dashed lines in Fig. 2 represent the results for YIG and YIG/Py, respectively. The simulation reproduces the decreasing trend of group velocities with magnetic field, which is consistent with spin waves in the dipolar regime [29]. The remaining discrepancies between the experiment and simulation might be attributed to the following aspects: (1) the exact pinning conditions and exchange constant, which can be strongly influenced by the quality of YIG/Py interface, are not known and (2) possibly a complex spin configuration might exist at the interface between YIG and Py at low magnetic fields [30].

In Figs. 4(a) and 4(b), we show the field dependence of spin-wave frequencies at $k_i = -0.5$ rad/μm. The numerically calculated values (open symbols) agree very well with the analytic formula (black line) in Fig. 4(a). Still, the measured frequencies (black symbols) show slight discrepancies, which might be attributed to a different gyromagnetic ratio in our sample compared to the literature value. The finite conductivity of the Py layer can also affect the frequency and intensity of spin-wave modes in the bilayer system [31–36]. Based on the analytic method in Ref. [31], we estimate the frequency shift of spin waves in YIG in the case of a 23-nm thick conductor mimicking Py. The shift amounts to less than 0.3 MHz at 24 mT (we assume $k < 0.5$ rad/μm and a conductivity of 7×10^6 S/m). This value is roughly three orders of magnitude smaller than the linewidth of YIG resonances induced by our CPW. Following this estimation, we did not take into account the conductivity of Py in our simulations.

Now we discuss the mode profiles simulated at 24 mT (Fig. 5). We display the values of m_y, that is, the dynamic magnetization component perpendicular to the film. The small amplitude variation along the y direction in Fig. 5(c) reflects the nonreciprocal character of the MSSW in a bare YIG film. While the PSSW1 in bare YIG has a perfectly antisymmetric profile [red curve in Fig. 5(c)], profiles of MSSW and PSSW1 in the YIG/Py bilayer are found to display a large asymmetry along the y direction [Fig. 5(d)]. Similar spin-wave-mode profiles were suggested in a recent work performed on a YIG/$Co_{40}Fe_{40}B_{20}$ bilayer system [14]. However, the impact on group velocities was not discussed. For the PSSW1 in YIG/Py, we also find spin

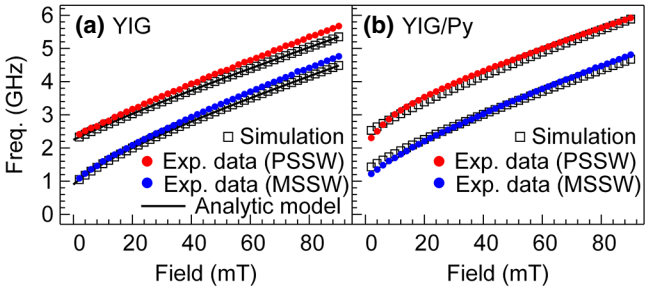

FIG. 4. Field dependence of MSSW and PSSW1 frequencies for (a) bare YIG and (b) YIG/Py bilayer. Blue and red dots are the frequencies extracted from measurement. The open black squares represent the results from the simulation. Black solid lines in (a) are results of the analytic formula in Ref. [28] for unpinned spins at boundaries.

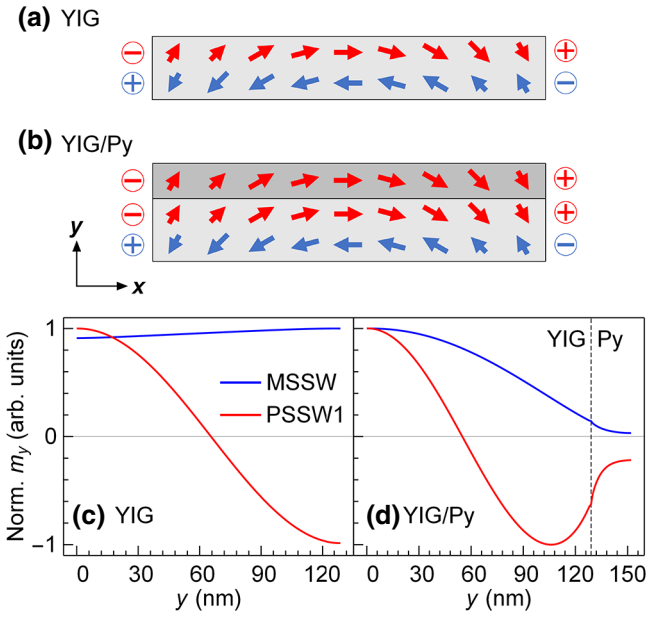

FIG. 5. Illustration of the spatial distribution of dynamic magnetization components for PSSW1 in (a) YIG and (b) YIG/Py. The induced magnetic charges are indicated by red and blue circles. The net magnetic charges cancel in (a) for YIG but not for (b) YIG/Py, creating a finite dynamic dipolar field. Simulated line profiles of $m_y(y)$ at 24 mT for (c) YIG and (d) YIG/Py. The blue and red solid lines represent MSSW and PSSW1, respectively. The black vertical dashed line in (d) indicates the boundary between YIG and Py. Maxima in $m_y(y)$ curves are normalized to one, thus facilitating the comparison.

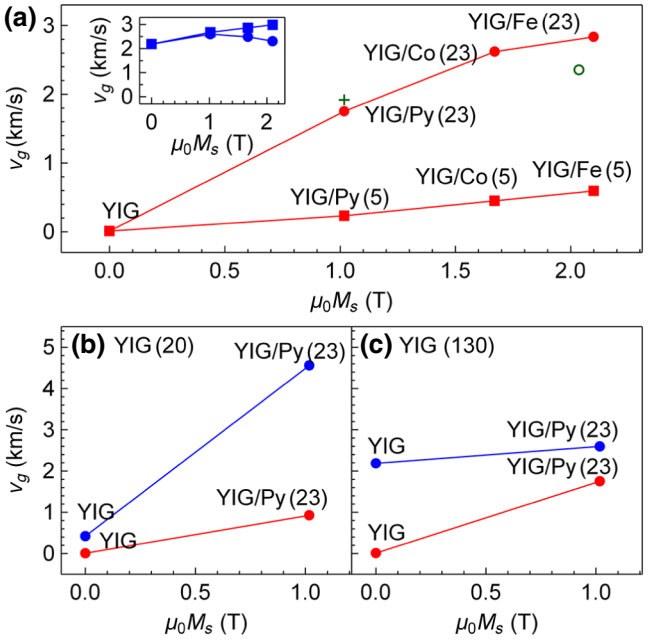

FIG. 6. (a) The simulated v_{PSSW1} for different magnetic metal top layers. The disks and squares represent bilayers with YIG thicknesses of 130 and 20 nm, respectively. The inset in (a) shows the corresponding v_{MSSW}. The cross and open circle represent the YIG/Py (23) with doubled exchange constant and doubled magnetization values, respectively. The group velocities for (b) 20-nm thick YIG and (c) 130-nm thick YIG are plotted for bare YIG and YIG/Py bilayer cases. The blue (red) symbols represent v_{MSSW} (v_{PSSW1}). The numbers in parentheses represent the layer thickness in nanometers.

precession in Py, not only in YIG. Though weak, the spin precession in Py is expected to alter the symmetry of the dynamic dipolar field in YIG. Figures 5(a) and 5(b) illustrate the dynamic magnetization components and induced magnetic charges. The net dipolar field due to the magnetic charges in YIG cancels out because of antiphase spin-precessional motion of the top and bottom segments of YIG [Fig. 5(a)]. The change in wave vector does not affect the cancellation effect. Therefore, the PSSW1 dispersion relation is flat. The situation is different for YIG/Py. The net dynamic dipolar field from the magnetic charges does not cancel out due to the intentionally added top layer of Py [Fig. 5(b)]. The dipolar field in PSSW1 for YIG/Py changes with wave vector similar to the MSSW in YIG [37]. Thus, v_{PSSW1} in YIG/Py depends on k and is increased.

V. DISCUSSION

Motivated by our experimental observations, we further explore different YIG/magnetic metal bilayer systems using our numerical simulation model. Figure 6(a) shows the simulation results of v_{PSSW1} with different magnetic metal layers on top of 130-nm thick (filled circles) and 20-nm thick YIG (filled squares). We note that the v_{PSSW1} greatly increases by the top magnetic layer while the v_{MSSW} increases only slightly or decreases. The thicker the magnetic metal layer, the more the v_{PSSW1} increases. Among the three magnetic layers, iron turns out to be the most effective material. The largest enhancement of 260 is found when adding 23-nm thick Fe to 130-nm thick YIG in Fig. 6(a). Two additional simulations are made in which we artificially modify the magnetic properties of Py: one with a doubled-exchange constant, A_{Py} (cross) and one with a doubled-saturation magnetization, M_{Py} (open circle) in Fig. 6(a). Compared to the original Py, there is an increase of a factor of 1.1 (1.3) for the case of the doubled A_{Py} (doubled M_{Py}). These results suggest that the magnetization M_{Py} of the top layer is more effective in increasing v_{PSSW1} than the exchange constant A_{Py}. Simulation results obtained for different YIG thicknesses provide further insights on the origin of the observed group velocity enhancement. We increase the frequency separation between the MSSW and PSSW1 branches by reducing the YIG thickness. For 20-nm thick bare YIG, PSSW1 lies in the 40 GHz range at 24 mT while MSSW still resides in the 2 GHz range, where v_{MSSW} is about 420 m/s [Fig. 6(b)]. This value is smaller than that in the 130-nm thick YIG

[Fig. 6(c)] as the group velocity scales with the thickness [38]. However, the v_{MSSW} increases significantly to about 4500 m/s when adding the top Py layer. The enhancement factor amounts to about 10 for v_{MSSW} and 100 for v_{PSSW1} when adding the 23-nm thick Py layer to 20-nm thick YIG [Fig. 6(b)]. This can be compared with Fig. 6(c) displaying the simulation results for 130-nm thick YIG. Here, v_{MSSW} increases by a factor of 1.2 while v_{PSSW1} increases by a factor of 170 when adding the Py layer to the 130-nm thick YIG. The result suggests that mode repulsion can contribute to the modification of group velocity. Overall, we suggest the hybridization of spin precessional motion in YIG and Py to enhance dipolar effects for magnetostatic modes and thereby increase their velocities. The enhanced dipolar interaction reported in this work is also advantageous to promote the recently presented concept of a directional coupler [39]. Here, dipolar effects between two separated but closely spaced YIG-based magnonic waveguides are key to providing an efficient coupling and optimum performance.

VI. CONCLUSION

In summary, we experimentally investigate the propagation characteristics of MSSW and PSSW in a YIG/Py bilayer and compare it with those of a bare 130-nm thick reference YIG film. Supported by simulations, we find that the PSSW group velocity in YIG/Py is significantly enhanced compared to that of the bare YIG. The spin-wave-mode profiles obtained from the numerical simulations suggest that the exchange coupling between YIG and Py causes the dynamic magnetization in Py to perform a forced precessional motion. This motion enhances dipolar effects for the resonant PSSW modes and their velocity. A significant enhancement of group velocities is also predicted for MSSWs in a bilayer of 20-nm thick YIG and 23-nm thick Py. This work paves the way to optimize bilayers for directional couplers and multifrequency magnonic devices, which provide multiple spin-wave modes propagating with high group velocities.

ACKNOWLEDGMENT

The research was funded by the EPFL COFUND Grant No. 665667 (EU Framework Programme for Research and Innovation (2014-2020), DU 1427/2-1 (Deutsche Forschungsgemeinschaft), Era.Net RUS Plus (TSMFA), and by SNSF via IZRPZ0_Grant No. 177550.

[1] A. Khitun, M. Bao, and K. L. Wang, Magnonic logic circuits, J. Phys. D **43**, 264005 (2010).
[2] A. Hoffmann and S. D. Bader, Opportunities at the Frontiers of Spintronics, Phys. Rev. Applied **4**, 047001 (2015).
[3] A. V. Chumak, A. A. Serga, and B. Hillebrands, Magnonic crystals for data processing, J. Phys. D **50**, 244001 (2017).
[4] A. A. Serga, A. V. Chumak, and B. Hillebrands, YIG magnonics, J. Phys. D **43**, 264002 (2010).
[5] B. Lenk, H. Ulrichs, F. Garbs, and M. Münzenberg, The building blocks of magnonics, Phys. Rep. **507**, 107 (2011).
[6] V. V. Kruglyak, S. O. Demokritov, and D. Grundler, Magnonics, J. Phys. D **43**, 264001 (2010).
[7] S. Neusser and D. Grundler, Magnonics: Spin waves on the nanoscale, Adv. Mater. **21**, 2927 (2009).
[8] D. Grundler, Reconfigurable magnonics heats up, Nat. Phys. **11**, 438 (2015).
[9] H. Yu, O. d' Allivy Kelly, V. Cros, R. Bernard, P. Bortolotti, A. Anane, F. Brandl, F. Heimbach, and D. Grundler, Approaching soft X-ray wavelengths in nanomagnet-based microwave technology, Nat. Commun. **7**, 11255 (2016).
[10] V. E. Demidov, M. P. Kostylev, K. Rott, J. Münchenberger, G. Reiss, and S. O. Demokritov, Excitation of short-wavelength spin waves in magnonic waveguides, Appl. Phys. Lett. **99**, 082507 (2011).
[11] Y. V. Khivintsev, L. Reisman, J. Lovejoy, R. Adam, C. M. Schneider, R. E. Camley, and Z. J. Celinski, Spin wave resonance excitation in ferromagnetic films using planar waveguide structures, J. Appl. Phys. **108**, 023907 (2010).
[12] A. Navabi, C. Chen, A. Barra, M. Yazdani, G. Yu, M. Montazeri, M. Aldosary, J. Li, K. Wong, Q. Hu, J. Shi, G. P. Carman, A. E. Sepulveda, P. Khalili Amiri, and K. L. Wang, Efficient Excitation of High-Frequency Exchange-Dominated Spin Waves in Periodic Ferromagnetic Structures, Phys. Rev. Applied **7**, 034027 (2017).
[13] S. Klingler, V. Amin, S. Geprägs, K. Ganzhorn, H. Maier-Flaig, M. Althammer, H. Huebl, R. Gross, R. D. McMichael, M. D. Stiles, S. T. B. Goennenwein, and M. Weiler, Spin-Torque Excitation of Perpendicular Standing Spin Waves in Coupled YIG/Co Heterostructures, Phys. Rev. Lett. **120**, 127201 (2018).
[14] H. Qin, S. J. Hämäläinen, and S. van Dijken, Exchange-torque-induced excitation of perpendicular standing spin waves in nanometer-thick YIG films, Sci. Rep. **8**, 5755 (2018).
[15] N. Vukadinovic, J. Ben Youssef, V. Castel, and M. Labrune, Magnetization dynamics in interlayer exchange-coupled in-plane/out-of-plane anisotropy bilayers, Phys. Rev. B **79**, 184405 (2009).
[16] J. Ben Youssef, V. Castel, N. Vukadinovic, and M. Labrune, Spin-wave resonances in exchange-coupled Permalloy/garnet bilayers, J. Appl. Phys. **108**, 063909 (2010).
[17] A. Papp, W. Porod, and G. Csaba, Hybrid yttrium iron garnet-ferromagnet structures for spin-wave devices, J. Appl. Phys. **117**, 17E101 (2015).
[18] C. Dubs, O. Surzhenko, R. Linke, A. Danilewsky, U. Brückner, and J. Dellith, Sub-micrometer yttrium iron garnet LPE films with low ferromagnetic resonance losses, J. Phys. D **50**, 204005 (2017).
[19] V. Vlaminck and M. Bailleul, Spin-wave transduction at the submicrometer scale: Experiment and modeling, Phys. Rev. B **81**, 014425 (2010).

[20] S. Neusser, G. Duerr, H. G. Bauer, S. Tacchi, M. Madami, G. Woltersdorf, G. Gubbiotti, C. H. Back, and D. Grundler, Anisotropic Propagation and Damping of Spin Waves in a Nanopatterned Antidot Lattice, Phys. Rev. Lett. **105**, 067208 (2010).

[21] M. Bailleul, D. Olligs, and C. Fermon, Propagating spin wave spectroscopy in a permalloy film: A quantitative analysis, Appl. Phys. Lett. **83**, 972 (2003).

[22] S. Klingler, A. V. Chumak, T. Mewes, B. Khodadadi, C. Mewes, C. Dubs, O. Surzhenko, B. Hillebrands, and A. Conca, Measurements of the exchange stiffness of YIG films using broadband ferromagnetic resonance techniques, J. Phys. D **48**, 015001 (2015).

[23] C. H. Bajorek and C. H. Wilts, Evidence for partial surface spin pinning in ferromagnetic resonance, J. Appl. Phys. **42**, 4324 (1971).

[24] J. P. Nibarger, R. Lopusnik, Z. Celinski, and T. J. Silva, Variation of magnetization and the Landé g factor with thickness in Ni–Fe films, Appl. Phys. Lett. **83**, 93 (2003).

[25] T. Schneider, A. A. Serga, T. Neumann, B. Hillebrands, and M. P. Kostylev, Phase reciprocity of spin-wave excitation by a microstrip antenna, Phys. Rev. B **77**, 214411 (2008).

[26] See Supplemental Material at http://link.aps.org/supplemental/10.1103/PhysRevApplied.11.034065 for the decay length analysis.

[27] H. Yu, O. d'Allivy Kelly, V. Cros, R. Bernard, P. Bortolotti, A. Anane, F. Brandl, R. Huber, I. Stasinopoulos, and D. Grundler, Magnetic thin-film insulator with ultra-low spin wave damping for coherent nanomagnonics, Sci. Rep. **4**, 6848 (2015).

[28] B. A. Kalinikos and A. N. Slavin, Theory of dipole-exchange spin wave spectrum for ferromagnetic films with mixed exchange boundary conditions, J. Phys. C **19**, 7013 (1986).

[29] A. Krysztofik, H. Głowiński, P. Kuświk, S. Ziętek, L. E. Coy, J. N. Rychły, S. Jurga, T. W. Stobiecki, and J. Dubowik, Characterization of spin wave propagation in (111) YIG thin films with large anisotropy, J. Phys. D **50**, 235004 (2017).

[30] T. Seki, K. Utsumiya, Y. Nozaki, H. Imamura, and K. Takanashi, Spin wave-assisted reduction in switching field of highly coercive iron-platinum magnets, Nat. Commun. **4**, 1726 (2013).

[31] M. Mruczkiewicz and M. Krawczyk, Nonreciprocal dispersion of spin waves in ferromagnetic thin films covered with a finite-conductivity metal, J. Appl. Phys. **115**, 113909 (2014).

[32] E. N. Beginin, Y. A. Filimonov, E. S. Pavlov, S. L. Vysotskii, and S. A. Nikitov, Bragg resonances of magnetostatic surface spin waves in a layered structure: Magnonic crystal-dielectric-metal, Appl. Phys. Lett. **100**, 252412 (2012).

[33] S. R. Seshadri, Surface magnetostatic modes of a ferrite slab, Proc. IEEE **58**, 506 (1970).

[34] I. S. Maksymov and M. Kostylev, Impact of conducting nonmagnetic layers on the magnetization dynamics in thin-film magnetic nanostructures, J. Appl. Phys. **113**, 043927 (2013).

[35] M. Mruczkiewicz, M. Krawczyk, G. Gubbiotti, S. Tacchi, Y. A. Filimonov, D. V. Kalyabin, I. V. Lisenkov, and S. A. Nikitov, Nonreciprocity of spin waves in metallized magnonic crystal, New J. Phys. **15**, 113023 (2013).

[36] J. Trossman, J. Lim, W. Bang, J. B. Ketterson, C. C. Tsai, and S. J. Lee, Effects of an adjacent metal surface on spin wave propagation, AIP Adv. **8**, 056024 (2018).

[37] M. J. Hurben and C. E. Patton, Theory of magnetostatic waves for in-plane magnetized anisotropic films, J. Magn. Magn. Mater. **163**, 39 (1996).

[38] A. G. Gurevich and G. A. Melkov, *Magnetization Oscillations and Waves* (CRC Press, New York, 1996).

[39] Q. Wang, P. Pirro, R. Verba, A. Slavin, B. Hillebrands, and A. V. Chumak, Reconfigurable nanoscale spin-wave directional coupler, Sci. Adv. **4**, e1701517 (2018).